ELSEVIER

Biochimica et Biophysica Acta 1232 (1995) 43–51

BBA Biochimica et Biophysica Acta

EPR study of trapped tyrosine Z^+ in Ca-depleted Photosystem II

Yoshio Kodera [a,1], Hideyuki Hara [a], Andrei V. Astashkin [a,2], Asako Kawamori [a,*], Taka-aki Ono [b]

[a] *Faculty of Science, Kwansei Gakuin University, Uegahara 1-1-155, Nishinomiya 662, Japan*
[b] *Solar Energy Research Group, Institute of Physical and Chemical Research (RIKEN), Wako 351-01, Japan*

Received 13 January 1995; revised 23 May 1995; accepted 29 June 1995

Abstract

The dependence of the light-induced transient EPR signal intensity of Y_Z^+ on the illumination temperature was measured in Ca-depleted PS II in the presence of DCMU. The maximum yield of Y_Z^+, about 70% of Y_D^+ EPR intensity, was obtained by illumination at 245 K. and trapped by immediate freezing in liquid nitrogen. Analysis of the relative intensities of Y_Z^+ and modified multiline EPR signals under various illumination periods and temperatures shows that Y_Z^+ has been trapped in the S_1 state of the oxygen evolving center, and the trapped Y_Z^+ EPR converted to the multiline signal through the advancement from the S_1 to S_2 state in the dark at 273 K. Spin-lattice relaxation times of Y_D^+ and Y_Z^+ in the Ca-depleted and Mn-depleted PS II were measured by pulsed EPR. From the relaxation enhancements of these radicals due to the dipole interaction with the Mn cluster, the distance from Y_Z^+ to the Mn cluster was estimated to be 15–20 Å. Using the 2 + 1 ESE method, the distance between Y_Z^+ and Y_D^+ was determined to be 29–30 Å.

Keywords: Photosystem II; Tyrosine; Calcium-depleted Photosystem II; EPR, pulsed; Spin-lattice relaxation

1. Introduction

The primary photochemical event in PS II is a charge separation between the reaction center chlorophyll P680 and the acceptor quinone Q_A. The oxidized P680 is then reduced by a redox-active tyrosine residue Y_Z within 20–250 ns [1]. Y_Z^+ is in turn reduced by an electron delivered from the Mn cluster in OEC with a halftime between 30 μs and 1500 μs, depending on the oxidation state of the Mn cluster [2]. Another redox-active tyrosine residue, Y_D, is functional as an auxiliary electron donor to $P680^+$, although it is not essential for the normal electron transport in PS II.

With a sequential absorption of photons by P680, the OEC cycles through five oxidation states, S_0 to S_4 [3], with release of one O_2 molecule in each cycle. In the S_2 state, the so-called multiline EPR signal of the Mn cluster in OEC is observed at cryogenic temperatures [4]. It has been extensively studied to elucidate the mechanism of the oxygen evolution and the molecular organization of the OEC as reviewed in [5].

The easily observable EPR signal of Y_D^+ has been used to establish the molecular structure and the location of this species in PS II [6]. The distance of 28–43 Å [7] or 23–28 Å [8] between Y_D and the Mn cluster in OEC was found from the analysis of the contribution of their dipolar interaction to the spin-lattice relaxation rate of Y_D^+. Later, using a pulsed EPR selective hole-burning method, this distance was estimated to be 28–30 Å [9]. The latter estimate is more reliable, since it is not derived from a relaxation equation but obtained by a direct spectroscopic measurement of the hole broadening induced by the dipole interaction of Y_D^+ and the Mn cluster. Another estimate for the distance with its direction from Y_D^+ to the Mn-cluster has recently been presented by Un et al. [10] by using a

Abbreviations: PS II, Photosystem II; Chl, chlorophyll; Cyt, cytochrome; P680, primary electron donor in Photosystem II; Y_Z, tyrosine-161 in the D1 subunit of PS II; Y_D, tyrosine-161 in the D2 subunit of PS II; Q_A, the primary electron acceptor in PS II; OEC, oxygen-evolving center; Mes, 2-morpholinoethanesulfonic acid; Mops, 4-morpholinopropanesulfonic acid; DCMU, 3-(3,4-dichlorophenyl)-1,1-dimethylurea; m.w. microwave; ESE, electron spin echo; CW, continuous wave.

* Corresponding author. Fax: +81 798 510914.
[1] Present address: School of Science, Kitasato University, Sagamihara 228, Japan.
[2] On leave from Institute of Chemical Kinetics and Combustion, Russian Academy of Sciences, 630090 Novosibirsk, Russia.

SSDI 0005-2728(95)00108-5

selective angular enhancement of the dipolar relaxation observed at 245 GHz EPR to be 25–35 Å.

The location of Y_D was evaluated to be 26 Å from the outer and 27 Å from the inner surface of the PS II membrane [11]. The distances from the outer and inner surfaces were also determined to be 36 Å and 20 Å, respectively [12]. The distance of 37 ± 5 Å from Y_D to the quinone-iron complex on the acceptor side of PS II has been estimated in [13,14]. In addition, the distances of 14 Å from Y_D and Y_Z to P680 have been predicted from a protein sequence analysis and using a homology between PS II and the photosystem of purple bacteria [15].

Though Y_Z is one of the most important redox components in PS II, information about its position in the membrane is quite limited. Though the distance between Y_Z and Mn cluster is still a matter of large debate, it is difficult to accumulate a Y_Z^+ state because of a rapid electron delivery from the Mn-cluster in the normal oxygen-evolving PS II. Tris-washing can remove most of Mn from PS II with inactivation of OEC [16]. In Mn-depleted PS II, Y_Z^+ can be trapped by immediate freezing in liquid nitrogen after illumination at 253 K [17]. This enabled us to measure its EPR spectrum with an improved signal-to-noise ratio and the spin-lattice relaxation time T_1 below 200 K. In addition, the distance of 30 Å between Y_Z^+ and Y_D^+ in Mn-depleted PS II was determined using the 2 + 1 ESE method [18]. Y_Z^+ can be trapped also in a mutant of cyanobacterium *Synechocystis* sp. PCC 6803, in which site-directed mutagenesis of the Y_D residue was carried out, and the distance from Y_Z to the non-hem iron has recently been determined to be the same as that from Y_D [19].

When PS II membranes are treated by a low-pH buffer, O_2 evolution activity is inhibited due to the removal of one Ca^{2+} indispensable for O_2 evolution, but the Mn-cluster and the extrinsic proteins are retained intact. In the treated membranes, the threshold temperature of the transition from the S_1 to the S_2 state is markedly upshifted as observed by thermoluminescence study [20] and a considerably high yield of Y_Z^+ EPR can be obtained during illumination at a temperature above 220 K in the absence of DCMU.

In this work we studied the temperature dependence of the reduction kinetics of Y_Z^+ in low-pH treated PS II membranes by a time-resolved EPR. We were able to trap Y_Z^+ by immediate freezing in liquid nitrogen after the illumination at the optimum temperature, when the electron donation from the Mn cluster is retarded. The trapped Y_Z^+ radical was then studied by pulsed EPR to provide information about the distance from this tyrosine residue to other electron carriers in PS II.

2. Materials and methods

The oxygen-evolving PS II membranes were prepared from spinach using the method of Berthold, Babcock and Yocum [21] with modifications described in [22]. The membranes were washed twice with 400 mM sucrose, 20 mM NaCl and 40 mM Mes/NaOH (pH 6.5), and resuspended in the same buffer. For Ca^{2+} depletion, the membranes at a Chl concentration of 0.5 mg/ml were suspended in a buffer; 400 mM sucrose, 20 mM NaCl, 10 mM citrate NaOH (pH 3.0) at 0°C for 5 min. Then, 10% vol. of the buffer; 400 mM sucrose, 20 mM NaCl and 500 mM Mops/NaOH (pH 7.5) were added to adjust the final pH at about 6.5, as described in [23,24]. The treated membranes were washed and, after centrifugation at 35 000 × g, resuspended in a final buffer of 20 mM NaCl, 0.5 mM EDTA and 40 mM Mes/NaOH (pH 6.5) with 50% vol. glycerol added. To ensure a single turnover of PS II, 50 μM DCMU was added to all samples. All procedures were carried out under complete darkness or dim green light to minimize any accidental excitation of PS II.

For Mn depletion, the membranes with a Chl concentration of 0.2–0.3 mg/ml were suspended in 0.8 M Tris buffer (pH 8.5) and stirred for 30 min at 277 K under the room light. The membranes were collected by centrifugation at 35 000 × g for 20 min and resuspended in the same final buffer as the Ca-depleted membranes. Final Chl concentrations were about 5 mg/ml for Ca-depleted and 7 mg/ml for Mn-depleted membranes.

For EPR measurements, 50 μM DCMU was always added to the membranes in order to ensure a single photochemical event in PS II, and then the membranes were transferred into Suprasil quartz tubes with the inner diameter of 4 mm. The sample tubes were sealed after purged by Ar gas. For time-resolved CW EPR experiments, the membranes were loaded into the flat Suprasil quartz tubes with a thickness of 1 mm and a height of 6 mm to ensure light saturation. Both types of sample were stored in liquid nitrogen pending measurement.

CW EPR measurements were performed on a Bruker ESP300E spectrometer. Microwave saturation characteristics were measured on each differently treated sample and a low microwave power selected to avoid saturation of the EPR signals of both tyrosines. The time resolution of the EPR signal kinetics measurements was 10 ms. A TE_{011} mode cylindrical cavity with an illumination window of 6 mm diameter was used for the measurements above 80 K. For the measurements at 6 K, a standard TE_{102} rectangular cavity with an Oxford ESR-900 helium gas-flow cryostat was used. A capillary with Cr^{3+}-doped MgO (g = 1.9800) was set inside the cavity as a reference for the calibration of signal intensity, resonance field and m.w. power. For Y_Z^+ trapping, illumination by a 500 W tungsten-Br_2 lamp was carried out through a 5 cm thick water layer and Kenko SR60 filters in a temperature-controlled transparent cryostat. In time-resolved experiments, an optical fiber connected to the cavity window and a camera shutter was used to control the illumination period.

Pulsed EPR experiments were performed on a Bruker ESP380 spectrometer equipped with a cylindrical dielectric

cavity (ER4117DLQ-H, Bruker) and a helium gas-flow system (CF935 Oxford Instruments). Spin-lattice relaxation rates were measured at 80 K using the saturation recovery technique, with a saturation sequence of five 90° (16 ns) pulses and a detection sequence of 90° (16 ns) and 180° (24 ns) pulses. 4 ms pulse repetition time was selected to ensure the complete magnetization recovery. The 2 + 1 ESE experiments were done at the temperature of about 5 K in a way similar to those described in [18]. Data analysis after experiments was done by a NEC PC9821 computer on the data transferred from a Bruker computer attached to the spectrometer.

3. Results and discussion

The light-induced EPR signal of Y_Z^+ in Ca-depleted PS II was studied by time-resolved CW EPR in the presence of DCMU. The kinetics obtained at 245 K and 273 K are shown in Fig. 1 by traces a and b, respectively. The signal intensity was monitored at the lower-field peak indicated by an arrowhead on the Y_D^+ EPR spectrum in the inset. The peak intensity reaches a maximum value I_{max} in about 5 s after the start of illumination. Then, even during illumination at 245 K, it decreases with a time constant of the order of hundreds of seconds. After switching the light off (dashed line in Fig. 1), about 25% of the current signal intensity at 245 K drops very quickly. The remaining 70–80% of the intensity exhibits a slow decay with a time constant of the order of hundreds of seconds. During about 10 min of dark relaxation, the intensity reaches a constant level, I_D, corresponding to the Y_D^+ EPR signal intensity at this magnetic field. At 273 K, however, the intensity decreases to I_D level within several seconds already during illumination in the presence of DCMU.

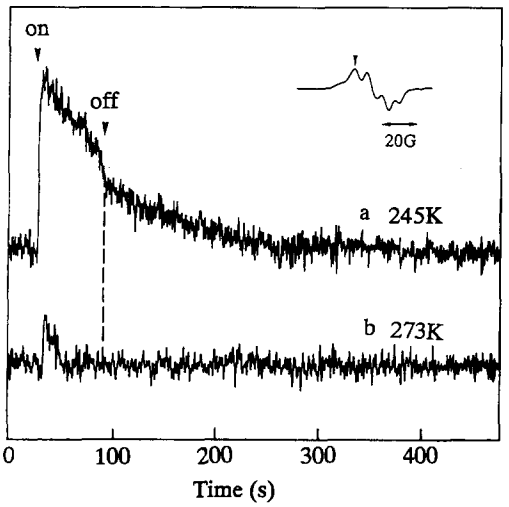

Fig. 1. The EPR signal kinetics measured at the illumination temperature of 245 K (a) and 273 K (b), at a magnetic field corresponding to $g = 2.0058$, as indicated by an arrowhead in the inset showing the EPR spectrum of Y_D^+. The illumination was turned on and off using a camera shutter. EPR conditions: m.w. frequency, 9.24 GHz; m.w. power, 0.8 mW; modulation frequency, 100 kHz; modulation amplitude, 2.5 G.

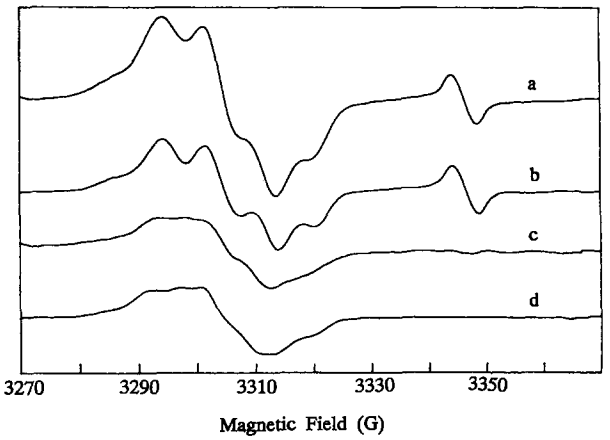

Fig. 2. EPR signals of Y_D^+ and Y_Z^+ in Ca-depleted PS II measured at 110 K: (a) in the Y_Z^+-trapped state after illumination for 5 s at 245 K, (b) after dark adaptation of the same sample for 20 min at 273 K, (c) obtained by subtraction of (b) from (a). (d) shows an EPR spectrum of the trapped Y_Z^+ observed in Tris-washed PS II after illumination at 253 K. A chlorophyll-like radical signal overlaps at the center with its intensity about 5% of the total. The similar radical signal is also present in (c) with less intensity. EPR conditions are same as in Fig. 1 except for the m.w. power of 125 μW.

These results contrast with those obtained for the untreated PS II membranes, where Y_Z^+ EPR signal could not be generated by a constant illumination at any temperature because of a rapid electron donation from OEC to Y_Z^+ above 130 K and a competitive electron donation from Chl or other radicals to $P680^+$ below 130 K [25]. In the low-pH-treated PS II, thermoluminescence study [23] has shown that the threshold temperature of the $S_1 \rightarrow S_2$ transition is about 70 K higher than in the untreated PS II. In addition, EPR Sig. II_f [16] appeared because of slow rereduction of Y_Z^+ as observed at 288 K during illumination in the absence of DCMU [23]. Consequently, as follows from our time-resolved EPR experiments, the Y_Z^+ yield in the Ca-depleted PS II increases at the illumination temperature lower than 254 K, where the electron donation from the OEC becomes slower. These considerations are further supported by similar experiments with Mn-depleted PS II, where a constant high level of Y_Z^+ signal above 240 K is obtained due to the lack of the electron donation from OEC [17].

The slow kinetic of the Y_Z^+ decay after switching the light off at a low temperature (Fig. 1a) provides a possibility to trap Y_Z^+ radicals by freezing in liquid nitrogen immediately after illumination. As an example, Fig. 2a shows the EPR spectrum of the sample frozen in liquid nitrogen immediately after illumination for 5 s at 245 K. After the dark adaptation for 20 min at 273 K, the Y_Z^+ radicals decayed and only the EPR spectrum of Y_D^+ could be recorded (Fig. 2b). Fig. 2c shows the difference spectrum (a − b) that corresponds to the trapped Y_Z^+. One can

notice a somewhat different shape of the Y_Z^+ spectrum compared with that of Y_D^+. The line shape is a little different from that observed by Babcock and Sauer in chloroplasts [16], but quite similar to that observed by Debus et al. in the cyanobacterium mutant *Synechocystis* 6803 [26]. We have also found that the line shape of Y_Z^+ is easily affected by the pH of the buffer, as shown in Fig. 2d, which was observed in Tris-treated PS II at pH 6.5 in the presence of DCMU after illumination at 253 K and different from that observed at pH 6.8 [17,18]. The tyrosine radicals in biological systems show a variety of EPR spectrum shapes [16,17,27,28]. This is determined mainly by the hyperfine splitting due to one of the β-methylene protons, which in turn reflects the dihedral angle of its bond to the methylene carbon and the ring plane [17,27]. Furthermore, the hydrogen bonding with a neighboring amino acid affects the spin density of the phenol oxygen of Y_D^+, resulting in a change of *hfs* of the ring protons [27,28].

The area of the Y_Z^+ signal obtained by double integration of Fig. 2c is about 70% of that of the Y_D^+ signal in Fig. 2b, which corresponds to the yield of trapped Y_Z^+. Using the signal shape shown in Fig. 2c and kinetics observed at the magnetic field position in Fig. 1, the yield of Y_Z^+ can be evaluated as $1.5(I_{max} - I_D)/I_D$. The factor of 1.5 takes into account a difference between the line shapes of Y_D^+ and Y_Z^+ seen in Fig. 2, where we determined the intensity I by the peak height. To investigate the temperature dependence of the Y_Z^+ yield, we assumed no temperature dependence of the line shapes of both tyrosines. To justify this assumption, we obtained the difference spectra from those observed during illumination at 253 K and after 20 min dark adaptation of the illuminated sample of Tris-treated PS II. We found no significant difference in the line shape of Y_Z^+ EPR from that obtained for the Y_Z^+ trapped sample at 77 K (data not shown). Actually, a chlorophyll-like EPR signal overlaps at the center, and this distorts the lineshape as shown in Fig. 2d. Further, the signal-to-noise ratio is worse on measurement at 253 K compared to that observed at 110 K (Fig. 2d). The dependence of the Y_Z^+ yield, normalized by Y_D^+ yield measured by EPR in the same sample, on the illumination temperature obtained is shown in Fig. 3. One can see that the maximum Y_Z^+ yield can be attained by the illumination at 245 K. Combining this result with the kinetics presented in Fig. 1a, we found that the maximum amount of Y_Z^+ can be trapped by immediate freezing after about 5 s illumination at 245 K. Following this procedure, we were able to trap as much as 70% of Y_Z^+ (see Fig. 2)

Since only a single electron transfer event in PS II is allowed in the presence of DCMU, it is reasonable to suppose that the OEC remains in the S_1 state in the PS II membranes with trapped Y_Z^+. In order to confirm this supposition, we quantitated the Y_Z^+ and Mn multiline EPR signals in the samples illuminated for various periods at several temperatures. Fig. 4 shows the result of measure-

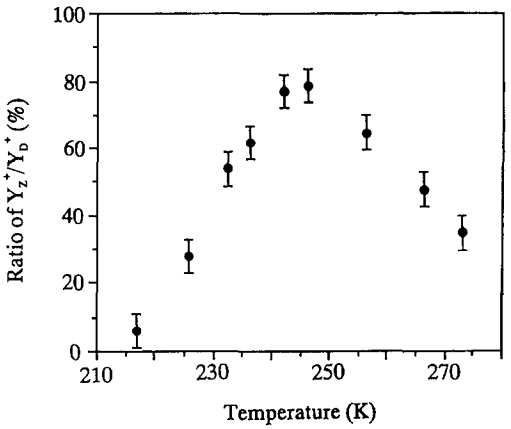

Fig. 3. The dependence of the Y_Z^+ yield on the illumination temperature. The yield was calculated from the maximum intensity of the Y_Z^+ signal intensity during illumination by assuming that the line shapes of both radicals do not change with temperature (see Fig. 1 and text).

ments of trapped Y_Z^+ EPR observed at 110 K (panel A) and the multiline signal observed at 6 K (panel B), respectively, on the several samples, using two spectrometers.

Before illumination no S_2 state has been formed over 5% noise level, as observed in Fig. 4Ba. In Fig. 4Aa the subtracted signal before illumination from that after the dark incubation is also shown. An intense Y_Z^+ signal was observed after the illumination for 5 s (Fig. 4Ac), while the intensity of the multiline signal (Fig. 4 Bc) in the same sample was much smaller than that induced by the illumination of a different sample at 273 K (Fig. 4Bb), when almost all OEC advanced to the S_2 state. Note that no Y_Z^+ was trapped after the illumination at 273 K (Fig. 4Ab). A weak narrow signal visible in this trace is attributed to a different radical produced by illumination [25]. With increasing the illumination period at 245 K, the intensity of the trapped Y_Z^+ signal decreased and, accordingly, a stronger multiline signal was induced (Fig. 4Bd and Be). After the dark incubation of the illuminated sample observed in Ac and Bc for 20 min at 273 K, the Y_Z^+ EPR signal disappeared completely (Fig. 4Af) and the multiline signal further increased to full intensity (Fig. 4Bf). This result suggests that during the dark incubation the trapped Y_Z^+ oxidizes the OEC in the S_1 state to form the S_2 state, resulting in the formation of Mn multiline and the disappearance of the Y_Z^+ signal. The overlapped signals around the center of Y_D^+ in Fig. 6Bc-Be may be ascribed to the S3 signal [29], which might be produced in the centers accidentally deficient of DCMU. However, its quantity can be estimated to be less than 5% of the Y_D^+ signal intensity and it will be neglected in further discussion.

Fig. 5 shows the relation between the yield of trapped Y_Z^+ and the multiline EPR signals in several samples under various illumination periods and temperatures. 100% Mn multiline intensity was assumed after the dark incubation (Fig. 4 Bf) of the illuminated sample (Fig. 4 Bc) and marked by f as the standard. Points marked by b to f were

taken from Fig. 4 and others without marks were obtained in the frozen samples with different illumination conditions; after illumination for 5 or 10 s at 250 or 260 K. The yields of Y_Z^+ signals in Fig. 5 were normalized by those of the Y_D^+ signals observed after dark incubation for 20 min at 273 K in the same sample. The yields of multiline signals were obtained from the total peak heights of five lines, as shown by arrowheads in Fig. 4Bb, divided by those after the dark incubation of the same illuminated sample.

One can see a negative linear relation between the amounts of trapped Y_Z^+ and of the OEC in the S_2 state, with 100% of the trapped Y_Z^+ corresponding to 0% of the S_2 state and 100% of the S_2 state corresponding to 0% of Y_Z^+. This relation proves that OEC remains in the S_1 state in the PS II membranes with trapped Y_Z^+, and that practically no other redox components are stably oxidized at the donor side of PS II during illumination at 245 K (see Fig. 2c). If less than 100% of Y_Z^+ is trapped, the sample consists of a mixture of the membranes in the S_1 (those with trapped Y_Z^+) and S_2 (those with Y_Z reduced and the multiline signal) states. The results obtained from this relation after illumination and trapping of Ca-depleted PS II in the presence of DCMU are summarized in the following scheme:

$$S_1Y_ZY_D^+Q_A \text{ (100\% } S_1 \text{ state)}$$
$$\downarrow \text{ illumination and trapping } \downarrow$$
$$S_1Y_Z^+Y_D^+Q_A^- \text{ (}p\text{\% } Y_Z^+\text{-trapped), } S_2Y_ZY_D^+Q_A^- \text{ (100-}p\text{\% } S_2 \text{ state)}$$
$$\downarrow \text{ dark incubation } \downarrow$$
$$S_2Y_ZY_D^+Q_A^- \text{ (100\% } S_2 \text{ state)}$$

(Scheme 1)

where p is a percentage of PS II membranes with trapped Y_Z^+.

Now let us consider the magnetic relaxation of Y_Z^+ in Ca-depleted PS II. The spin-lattice relaxation times T_1 of Y_Z^+ and Y_D^+ in Ca-depleted and Mn-depleted PS II membranes were measured at the temperature of 80 K using the saturation recovery method of pulsed EPR. The saturation recovery trace is simply described by the following expression:

$$V(t) \propto 1 - \exp(-t/T_1) \quad (1)$$

where $V(t)$ is an ESE amplitude obtained with a delay time t after the saturating pulse sequence. We will consider the spin-lattice relaxation rate of a radical to consist

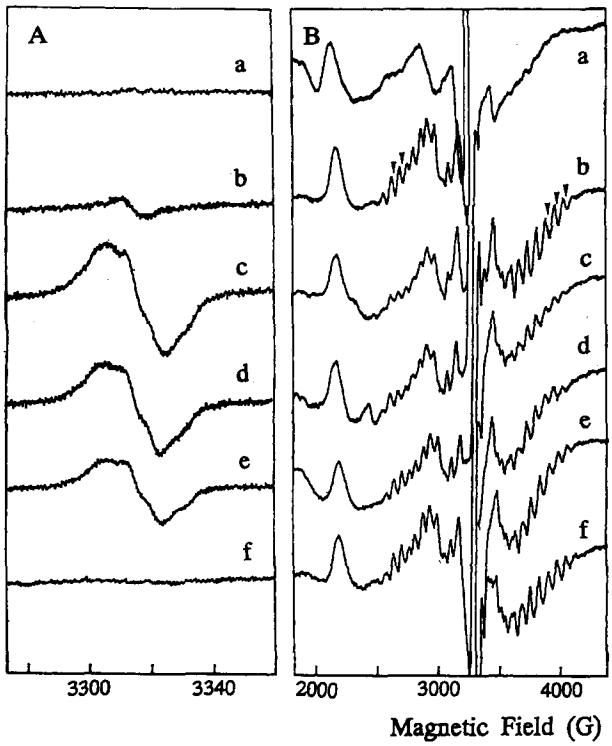

Fig. 4. The EPR signals of trapped Y_Z^+ measured at 110 K (Ab–Af) and modified Mn multiline signals observed at 6 K (Bb–Bf). Y_Z^+ was trapped by immediate freezing after illumination for 30 s at 273 K (b), for 5 s at 245 K (c), for 10 s at 245K (d) and for 20 s at 245 K (e). Spectra (Af) and (Bf) were measured after dark adaptation of the same sample for 20 min at 273 K, following the measurement of (Ac) and (Bc). (Aa) shows the spectrum Y_Z^+ observed before illumination subtracted by that after illumination and dark incubation at 273 K. (Ba) shows the spectrum observed at 6 K in the same sample before illumination in order to detect any S_2 signal. The lines indicated by arrowheads as shown in (Bb) will be used to calibrate the intensity of the multiline signal in each sample after background correction. The signal at about $g = 3.0$ in panel (B) is ascribed mostly to the oxidized low-potential Cyt b-559. EPR conditions for (A) are same as those in Fig. 2. EPR conditions for (B): m.w. frequency, 9.4 GHz; m.w. power, 0.8 mW; modulation frequency, 100 kHz; modulation amplitude, 20 G.

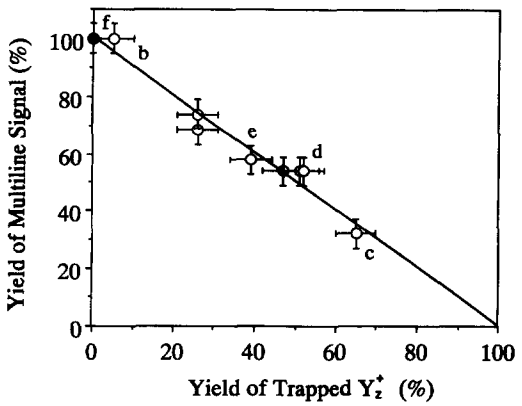

Fig. 5. The relation between the yields of the modified multiline signal and that of trapped Y_Z^+ after illumination for various periods at various temperatures. Circles b to f were obtained from Fig. 4 and others without marks were obtained from the samples under different illumination conditions (see text). The yield of Y_Z^+ signal was normalized by that of Y_D^+ after the dark incubation of the illuminated sample for 20 min at 273 K. Intensity of the multiline signal in each measurement was estimated from summation of the peak heights of five lines as indicated by arrowheads in Fig. 4Bb, and normalized by that after dark incubation of each illuminated sample, resulting the yield of Mn multiline. f marked by a closed circle is assumed to be 100% yield of the Mn multiline, as observed in Fig. 4Bf. The straight line was drawn by a least square fitting and it coincided with 100% of the Y_Z^+ yield.

of two terms: $1/T_l = (1/T_l)_{int} + (1/T_l)_d$, where $(1/T_l)_d$ is a contribution to the relaxation due to the dipole interactions of the radical with fast-relaxing transition metal ions that is anisotropic. $(1/T_l)_d$ may include several terms due to different sources. The intrinsic relaxation rate $(1/T_l)_{int}$ includes all other isotropic sources of the relaxation.

The dipole relaxation rate of a radical interacting with a paramagnetic ion can be expressed by the formula [13,19]:

$$(1/T_1)_d = W_m(S, \omega, \theta)/R^6 \quad (2)$$

where R is the distance between the ion and the radical. The factor W_m determines the efficiency with which the metal ion enhances the relaxation of the radical at a given distance. It is a function of spin S, θ, the orientation of the vector **R** with respect to the direction of the static magnetic field and ω, the resonance frequency of the radical [13]. The appropriate expression for W_m depends also on the values of the spin-lattice and spin-spin relaxation times of the metal ion (see, e.g., [13,14,19] and [30]). In a non-oriented system, the saturation recovery kinetics given

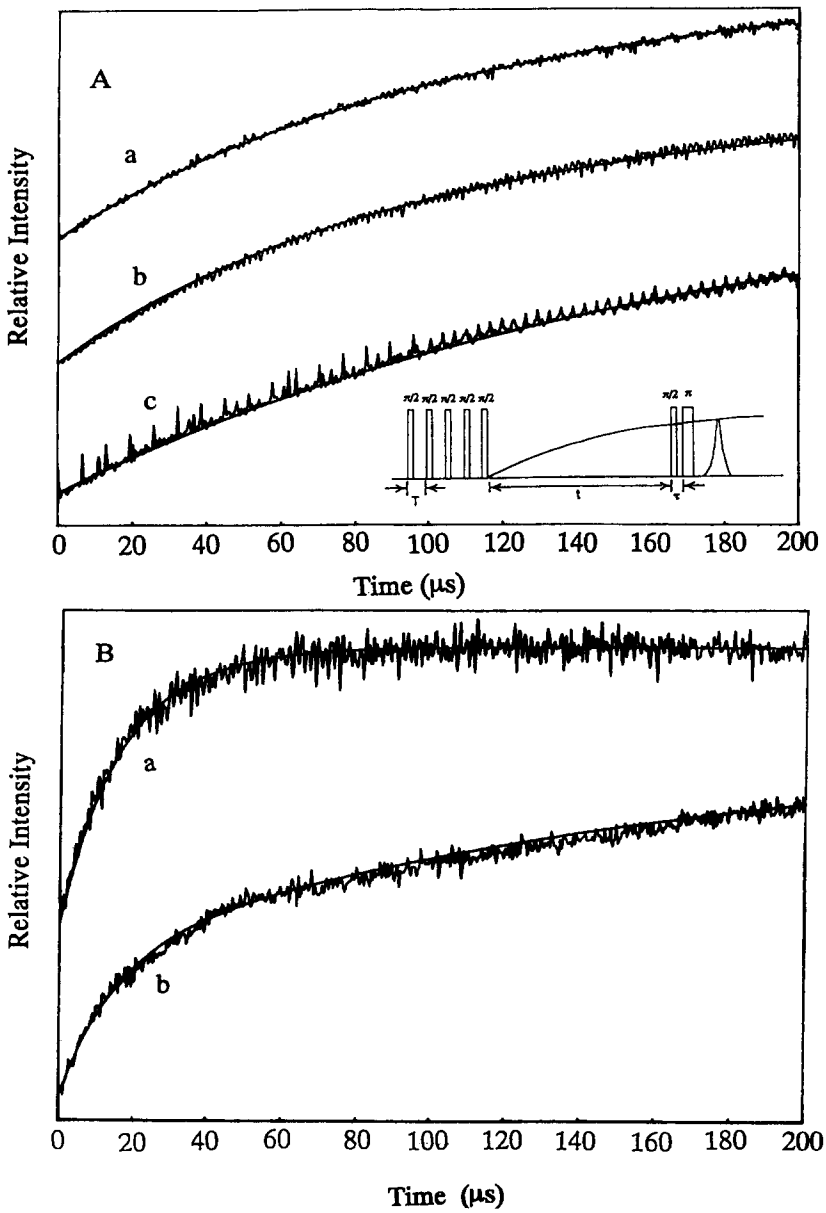

Fig. 6. (A) Saturation recovery kinetics of Y_D^+ recorded at 80K in Ca-depleted PS II in S_1 (before illumination) (a) and S_2 (after the dark incubation at 273 K for 20 min) (b) states and in Mn-depleted PS II (c). The inset shows the pulse train used for these measurements with the repetition time of 4 ms. (B) Saturation recovery kinetics of Y_Z^+; (a) in Ca-depleted PS II, derived from the experimental kinetics in the Y_Z^+ trapped state by subtracting the traces for Y_D^+ in S_1($p = 66\%$) and S_2(34%) states (see text). The trace (b) in Mn-depleted PS II was obtained by subtraction of the curve (Ac) of Y_D^+ from the saturation recovery obtained in the Y_Z^+ trapped state after illumination, using 60% for the ESE amplitude of Y_Z^+. This kinetics is fitted with the curve $[1 - (1/3) \cdot \exp[-t/22\ \mu s] - (1/3) \cdot \{\int \exp - \{k_d f(\theta)t + k't\} \sin\theta d\theta\}]$, using the parameters $k_d = 33 \cdot 10^3$ and $k' = 0.5 \cdot 10^3\ s^{-1}$ in Table 1.

by Eq. (1) is to be averaged over θ and this averaging generally does not result in any single-exponential saturation recovery kinetics [13,30].

Considering the theoretical expressions for $W_m(S, \omega, \theta)$ [13,30], we expect that the averaged value $\langle W_m(S, \omega)\rangle$ will be almost same for all radicals, whose g-factors and EPR line shape are not different. Therefore, we denote the common factor $k_d \times R^6$ in B or C terms [13] for the dipolar interaction with, for example, the Mn cluster, which does not include the angular variable, to be same for both tyrosine radicals in PS II. The immediate consequence of this consideration is that the ratio of distances from the Mn cluster to Y_Z^+ ($R_{Z,Mn}$) and to Y_D^+ ($R_{D,Mn}$) can be estimated as:

$$R_{Z,Mn}/R_{D,Mn} = \left[(k_{d,Mn})_D/(k_{d,Mn})_Z\right]^{1/6} \quad (3)$$

In experiment, the part of saturation recovery of the tyrosine caused by the Mn-cluster can be obtained from the recovery measured in Mn-sufficient (in our case, Ca-depleted) divided by that in Mn-deficient (Tris-washed) preparations of PS II, because of the multiplicative character of relaxation. The curve obtained by the division can be fit with the curves simulated over various k_d and k' values as given in [13,30]

$$1 - \exp(-k't) \cdot (1/2)\int \exp\left[-k_{d,Mn} f(\theta) t\right] \sin\theta \, d\theta \quad (4)$$

where $f(\theta) = \sin^2\theta\cos^2\theta$ for the C term and $k' = (1/T_1)_{int}$ is a contribution from the isotropic relaxation rate.

Fig. 6A shows the saturation recovery kinetics observed at 80 K for Y_D^+ in the Ca-depleted PS II in S_1 state (a) (before illumination) and S_2 (b) state (after the dark adaptation). Fig. 6Ac shows the saturation recovery kinetics observed in the Mn-depleted PS II. The relaxation rate due to the non-heme iron, $k_{d,Fe}$, can be determined from the simulation of Eq. (4) as shown by the best-fit solid curve. This curve is used to divide the recovering part of Fig. (Aa) to find $k_{d,Mn}$ in the same way. The best-fit values along with experimental ones are shown by a solid curve in Fig. 6Aa. The values of $k_{d,Mn}$, $k_{d,Fe}$ and k' thus determined for Y_D^+ in the S_1 state are presented in Table 1.

In the Y_Z^+-trapped sample, the saturation recovery kinetics is expected to consist of three components, corresponding to Y_Z^+ in the S_1 state (p%) and to Y_D^+ in the S_1(p%) and S_2 ($100-p$%) states. In Fig. 6Ba is shown the recovery trace Y_Z^+ in Ca-depleted PS II which was obtained by subtraction of Y_D^+ in S_1 state (Aa) (in proportion with the Y_Z^+ trapping yield $p = 66\%$) and S_2 state (Ab) (34%) from the trace measured in Y_Z^+ trapped state (data not shown).

In Fig. 6Bb are presented the saturation recovery kinetics obtained for the Y_Z^+ in the Mn-depleted PS II, with 60% Y_Z^+ trapped, after subtraction of Y_D^+ components (Fig. 6Ac). In contrast to the trace observed in Ca-depleted PS II (Fig. 6Ba), it consists of two components, with the contribution of the fast one being 30% of the total ESE signal intensity at $t \to \infty$ that can be measured by a usual two-pulse ESE sequence. This part corresponds to 1/3 of the Y_Z^+ yield measured by a CW EPR in the same sample, and cannot be considered to be due to all of Y_Z^+ radical. On the other hand, the slower component of Y_Z^+, about the remaining 70% recovered after a 20 μs delay, almost coincides with the kinetics of Y_D^+ in the same sample shown in Fig. 6Ac.

We investigated the cause of the deviation from the normal dipolar-type relaxation as follows. We first suspected the effect of retained Mn after Tris-treatment, and examined its content by an ICP mass spectrometer PE SCIEX model ELAN 5000. Only about $5 \cdot 10^{-3}$ manganese per reaction center based on Cyt b-559 content was detected using a standard stock solution of $1.00 \cdot 10^{-3}$ M Mn^{2+} dissolved in 0.3 M nitric acid. Next, an effect of Fe^{3+}, existing everywhere on earth, may be suspected. Saturation recovery kinetics of Tris-treated PS II with 100 μM $FeCl_3$ added was examined at 80 K after illumination in the same way. However, we could not observe any extra effect on the saturation recovery of Y_D^+ and Y_Z^+. The last plausible cause may be an effect of oxygen dissolved from air during treatment. We tried to trap oxygen gas into the sample by bubbling it about 30 s at room temperature and then the sample tube was sealed. The saturation recoveries observed at 80 K for this sample showed about 40% of a shorter relaxation component in both Y_Z^+ and Y_D^+. Thus, we found that the effect of trapped oxygen should not be neglected. Further studies of the oxygen effect on Y_D^+ relaxation kinetics are now in progress.

On the other hand, Y_D^+ saturation recovery in the Tris-treated PS II shown in Fig. 6Ac fits well with the curve simulated by Eq. (4), probably because Y_D^+ is located in a hydrophobic area or buried deep inside of PS II as suggested [15,32]. Low oxygen concentration in the ordinary Tris-treated PS II might not affect on the relax-

Table 1
Spin-lattice relaxation rates k ($\times 10^3$ s^{-1}) values at 80 K in Ca- and Mn-depleted PS II

Radical:	Y_D^+			Y_Z^+		
Sample	$k_{d,Fe}$	$k_{d,Mn}$	k_{int}	$k_{d,Fe}$	$k_{d,Mn}$	k_{int}
Ca-depleted PS II (S_1-state)	33	7	3	33	160	40
Mn-depleted PS II	33		0	33		0.5

k of Y_Z^+ in Mn-depleted PS II is found to be nearly equal to that of Y_D^+ (see discussion in the text). The relative error is estimated to be about 10%.

ation of Y_D^+. Similarly, in Ca-depleted PS II, oxygen trapping around Y_Z has been protected by the three extrinsic proteins. The values of $k_{d,Fe}$ for Y_D^+ and Y_Z^+ in Mn-depleted PS II coincide, which imply that the distance from the non-hem iron is same as shown in [19]. The kinetics in Fig. 6Bb were approximated by 70% dipolar and intrinsic type and 30% of a shorter isotropic relaxation component shown by the solid curve on it. Using the part with slow kinetics fitted with Fig. 6Bb for the division and after angular average of Eq. (4), the best-fit saturation recovery is shown by a solid curve on Fig. 6Ba. Thus, the value of $k_{d,Mn}$ obtained for the S_1 state in Ca-depleted PS II is also shown in Table 1 along with that of $k_{d,Fe}$.

Substituting the k_d values from Table 1 into Eq. (3), we estimate $R_{Z,Mn}/R_{D,Mn} = 0.60 \pm 0.06$. All the probable errors in experiments and calculations are included here. Thus, Y_Z is suggested to be closer to the Mn cluster in OEC than Y_D. This result is reasonable, since Y_Z is involved in the main electron transfer path and has significantly faster oxidation/reduction kinetics than Y_D. Assuming no change in distances between each tyrosine and the Mn-cluster after low-pH treatment, and using the value of 28–30 Å for $R_{D,Mn}$ previously obtained in [9], the distance between Y_Z and the Mn cluster is calculated to be 15.1–19.8 Å.

In the above estimate we did not take into account the influence of the dipole interaction between Y_D^+ and trapped Y_Z^+ on their spin-lattice relaxation rates. The relaxation times of the tyrosines of the order of several tens of microseconds are much longer than the values of the order of inverse resonance frequency (10^{-10} s) required to provide a substantial relaxation enhancement [7,8]. The difference in contribution of the acceptor iron in the initial and Y_Z^+-trapped states to Y_D^+ relaxation was also neglected, because the distance to this iron is relatively large ≈ 37 Å [13,14]. The effect of oxidized Cyt *b*-559 [31] on the spin-lattice relaxation of both tyrosine radicals was neglected, because we observed no remarkable change in the relaxation rate of Y_D^+ by a change in oxidation state of Cyt *b*-559 in our previous work [8]. In addition, the EPR signal intensities of the low potential Cyt *b*-559 [31] shown in Fig. 4Ba–Bf do not change noticeably, suggesting that the Cyt *b*-559 state was not altered by illumination.

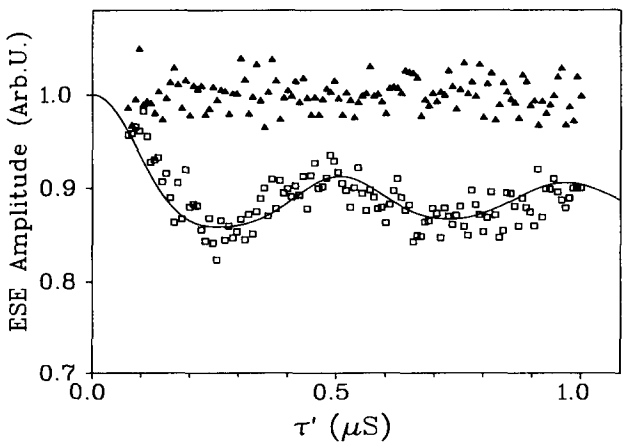

Fig. 7. The 2+1 ESE traces of tyrosine radicals in Ca-depleted PS II obtained at 4.2 K. Open squares: in the illuminated sample. Filled triangles: in the same sample after dark-adaptation. Solid line: calculated for the dipole interaction constant $D = 2.2$ MHz (see [18]). All traces are normalized to unity at $\tau' = 0$.

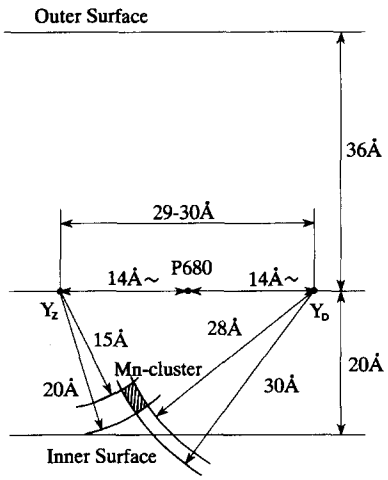

Fig. 8. Summary of the distance relations between Y_D, Y_Z, and the Mn-cluster. The position of P680 is assumed to lie in the middle of both tyrosines Y_Z and Y_D, but may have some ambiguity depending on a model for P680 (see text). The distances of Y_D (see Ref. [12]) and Y_Z from the membrane surfaces are assumed to be same.

The value of 15–20 Å is the first quantitative estimate of the distance between Y_Z and the Mn cluster. It does not contradict the value greater than 15 Å suggested in [33] on the basis that no appreciable broadening of Y_Z^+ spectrum by the Mn cluster is observed. The distance less than 10 Å proposed in [34] to explain the difference in the microwave saturation characteristics of Y_D^+ and Y_Z^+, is not supported by any quantitative analysis, as proved later by another group [35]. Mutagenesis studies of Asp-170 of the D1 polypeptide in *Synechocystis* 6803 suggest a rather short distance between Y_Z and the Mn cluster [36]. However, this result does not give any direct information about the distance. At least the result obtained here for Ca-depleted PS II suggests that the metal-binding center close to Y_Z^+, shown by a computer modeling [32], is not a paramagnetic metal ion.

In the Y_Z^+-trapped state, we used a 2 + 1 ESE method [37] to determine the dipole interaction between Y_D^+ and Y_Z^+. This experiment was essentially the same as that presented in [18] for the Mn-depleted PS II. The traces obtained in the Y_Z^+-trapped and dark-adapted states are shown in Fig. 7 by open squares and filled triangles, respectively. The low-frequency oscillation visible in the trace for the illuminated sample is caused by the dipole interaction between the tyrosines (for detailed consideration, see [18]). By the computer simulations, using the expression given in [18], the perpendicular component of the dipole interaction tensor was determined to be $D = 2.2$

± 0.1 MHz. The solid line in Fig. 7 is simulated for $D = 2.2$ MHz. This estimate agrees well with the value of about 2 MHz found in [18] for the Mn-depleted PS II and corresponds to the distance of 29–30 Å between the tyrosines. The quantitative agreement between the results for the Ca- and Mn-depleted PS II implies that no significant structural modification around the tyrosines results from the biochemical treatments involved.

The structural data obtained in this work and elsewhere [9] are summarized in Fig. 8. The position of the manganese cluster is consistent with the prediction by [33], closer to Y_Z than to Y_D. The assumed position of P680 is taken to be equal from the both tyrosines as shown by [15] and is also consistent with the suggestion of a distance greater than 15 Å from the Mn cluster in [38]. An ambiguity for this symmetric position of P680 may be suggested in a different model [39]. This model does not alter our conclusion about the distance between Y_Z^+ and the Mn cluster, if P680 is shifted in any direction other than to the Mn-cluster.

Acknowledgements

This work was supported by JSPS (Japan Society for the Promotion of Science) fellowships and funds to Y. Kodera and A.V. Astashkin. The authors are indebted to Professor Akabori of Hiroshima University for the analysis of the manganese content in Tris-treated PS II.

References

[1] Brettel, K., Schlodder, E. and Witt, H.T. (1984) Biochim. Biophys. Acta 766, 403–415.
[2] Saygin, O. and Witt, H.T. (1987) Biochim. Biophys. Acta 893, 452–469.
[3] Kok, B., Forbush, B. and McGloin, M. (1970) Photochem. Photobiol. 11, 456–475.
[4] Dismukes, G.C. and Siderer, Y. (1981) Proc. Natl. Acad. Sci. 78, 274–278.
[5] Debus, R.J. (1992) Biochim. Biophys. Acta 1102, 269–352.
[6] Barry, B.A., El-Deeb, M.K., Sandusky; P.O. and Babcock, G.T. (1990) J. Biol. Chem. 265, 20139–20143.
[7] Evelo, R.G., Styring, S., Rutherford, A.W. and Hoff, A.J. (1989) Biochim. Biophys. Acta 973, 428–442.
[8] Kodera, Y. Takura, K. and Kawamori, A. (1992) Biochim. Biophys. Acta 1101, 23–32.
[9] Kodera, Y., Dzuba, S.A., Hara, H. and Kawamori, A. (1994) Biochim. Biophys. Acta 1186, 91–99.
[10] Un, S., Brunel, L.-C., Brill, T.M., Zimmermann, J.-L. and Rutherford, A.W. (1994) Proc. Natl. Acad. Sci. USA 91 5262–5256.
[11] Innes, J.B. and Brudvig, G.W. (1989) Biochemistry 28, 1116–1125.
[12] Isogai, Y., Itoh, S. and Nishimura, M. (1990) 1017, 204–208.
[13] Hirsh, D.J., Beck, W.F., Innes, J.B. and Brudvig, G.W. (1992) Biochemistry 31, 532–541.
[14] Hirsch, D.J. and Brudvig, G.W. (1993) J. Phys. Chem. 97, 13216–13222.
[15] Svensson, B., Vass, I., Cedergren, E. and Styring, S. (1990) EMBO J. 9, 2051–2059.
[16] Babcock, G.T. and Sauer, K. (1975) Biochim. Biophys. Acta 376, 315–328.
[17] Kodera, Y., Takura, K., Mino, H. and Kawamori, A. (1992) in Research in Photosynthesis (Murata, N., ed.), Vol. II, pp. 57–60, Kluwer, Dordrecht.
[18] Astashkin, A.V., Kodera, Y. and Kawamori, A. (1994) Biochim. Biophys. Acta 1187, 89–93.
[19] Koulougliotis, D. Tang, X.-S., Diner B.A. and Brudvig, G.W. (1995) Biochemistry 34, 2850–2856.
[20] Ono, T. and Inoue, Y. (1990) Biochim. Biophys. Acta 1015, 373–377.
[21] Berthold, D.A., Babcock, G.T. and Yocum, C.F. (1981) FEBS Lett. 134, 231–234.
[22] Ono, T. and Inoue, Y. (1989) Biochim. Biophys. Acta 973, 443–449.
[23] Ono, T. and Inoue, Y. (1988) FEBS Lett. 227, 147–152.
[24] Ono, T. and Inoue, Y. (1992) Biochemistry 31, 7648–7655.
[25] De Paula, J.C., Innes, J.B. and Brudvig, G.W. (1985) Biochemistry 24, 8114–8120.
[26] Debus, R.J., Barry, B.A., Sithole, I., Babcock, G.T. and McIntosh, L. (1988) Biochemistry 27, 9071–9074.
[27] Hoganson, C.W. and Babcock, G.T. (1992) Biochemistry 31, 11874–11880.
[28] Tommos, C., Davidsson, L., Svensson, B., Madsen, K., Vermaas, W. and Styring, S. (1993) Biochemistry 32, 5436–5441.
[29] Bousac, A., Zimmermann, J.-L. and Rutherford, A.W. (1989) Biochemistry 28, 3476–3483.
[30] Evelo, R.G. and Hoff, A.J. (1991) J. Magn. Reson. 95, 495–508.
[31] Thomson, L.K., Miller, A.-F., Buser, C.A., De Paula, J.C. and Brudvig, G.W. (1989) Biochemistry 28, 8048–8056.
[32] Svensson, B., Vass, I. and Styring, S. (1991) Z. Naturforsh. 46c 765–776.
[33] Hoganson, C.W. and Babcock, G.T. (1988) Biochemistry 27, 5848–5855.
[34] Hallahan, B.J., Nugent, J.H.A., Warden, J.T. and Evans, M.C.W. (1992) Bichemistry 31, 4562–4573.
[35] Bousac A. and Rutherford, A.W. (1992) Biochemistry 31, 7441–7445.
[36] Nixon, P.J. and Diner, B.A. (1992) Biochemistry 31, 942–948.
[37] Kurshev, V.V., Raitsimring, A.M. and Tsvetkov, Yu.D. (1989) J. Magn. Reson. 81, 441–454.
[38] Hoganson, C.W. and Babcock, G.T. (1989) Biochemistry 27, 1448–1454.
[39] Van Mieghem, F.J.E., Satoh, K. and Rutherford, A.W. (1991) Biochim. Biophys. Acta 1058, 379–385.